

Magnetophoresis in the Rubinstein – Duke model

A. Drzewiński,¹ E. Carlon,^{2,3} and J.M.J. van Leeuwen⁴

¹*Institute of Low Temperature and Structure Research,
Polish Academy of Sciences, P.O. Box 1410, Wrocław 2, Poland*

²*Theoretische Physik, Universität des Saarlandes, D-66041 Saarbrücken, Germany*

³*Interdisciplinary Research Institute c/o IEMN, Cité Scientifique BP 69, F-59652 Villeneuve d'Ascq, France*

⁴*Instituut-Lorentz, Leiden University, P.O. Box 9506, 2300 RA Leiden, The Netherlands*

(Dated: November 21, 2018)

We consider the magnetophoresis problem within the Rubinstein – Duke model, i.e. a reptating polymer pulled by a constant field applied to a single repton at the edge of a chain. Extensive density matrix renormalization calculations are presented of the drift velocity and the profile of the chain for various strengths of the driving field and chain lengths. We show that the velocities and the average densities of stored length are well described by simple interpolating crossover formulae, derived under the assumption that the difference between the drift and curvilinear velocities vanishes for sufficiently long chains. The profiles, which describe the average shape of the reptating chain, also show interesting features as some non-monotonic behavior of the links densities for sufficiently strong pulling fields. We develop a description in which a distinction is made between links entering at the pulled head and at the unpulled tail. At weak fields the separation between the head zone and the tail zone meanders through the whole chain, while the probability of finding it close to the edges drops off. At strong fields the tail zone is confined to a small region close to the unpulled edge of the polymer.

PACS numbers: 47.50.+d, 05.10.-a, 83.10.Ka

I. INTRODUCTION

The magnetophoresis problems is a member of the class of reptation problems in which a long polymer is driven through a gel. The reptative motion of the polymer can be successfully modeled by a lattice version using sections of the polymer (the reptons) as the mobile units, which hop stochastically from cell to cell. The driving field is incorporated as a bias in the hopping rates, favoring the motion in the field direction. A simple and adequate model is the Rubinstein - Duke model [1], which represents the polymer as a chain of N independently moving reptons, with the restriction that the integrity of the chain is preserved. The reptons trace out a connected string of cells in space, each cell containing at least one repton. The cells, which can be multiply occupied, carry the extra reptons as units of stored length. In order to preserve the integrity of the chain, only those reptons which are located in cells with stored length can hop.

Usually one considers the case of polyelectrolytes in which the reptons are uniformly charged. Thus the driving field pulls equally on all reptons and the bias is the same for the hopping rates all along the chain. A practical situation where this occurs is in DNA electrophoresis [2]. The DNA molecules, being acid, get charged in solution and when they are placed in a gel subject to an external electric field they perform a biased reptative motion along the field direction. Electrophoresis is a technique of great importance in molecular biology and sequence analysis, as it allows to separate DNA strands according to their length [2].

In nature the charge distribution is of course not always uniform. The extreme alternative is the case where

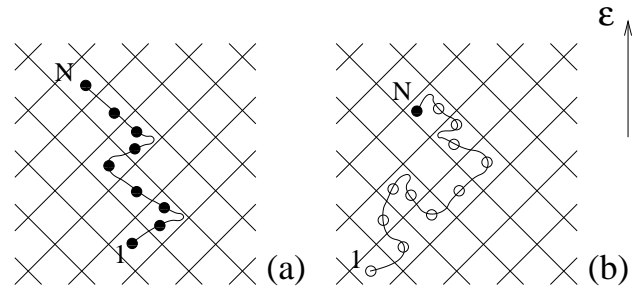


FIG. 1: Examples of configurations of reptating polymers in the Rubinstein – Duke model in the case of (a) Electrophoresis and (b) Magnetophoresis. Black reptons perform a biased motion along the direction of the applied field while white reptons are unbiased. The configuration for a chain with N reptons is given by a set of $N - 1$ integers $(y_1, y_2 \dots y_{N-1})$ measuring the distance of two neighboring reptons along the field direction (thus $y_i = 0, \pm 1$). For the two examples shown the coordinates are $(1, 0, 1, 1, 1, 0, 1, 1)$ for (a) and $(1, 1, 1, 0, -1, 1, 1, 1, 0, 1, 0)$ for (b).

all reptons are neutral except one end repton, which is charged. A possible realization of such a situation is a magnetic bead, attached at one end of the polymer, which is driven by a magnetic field. Therefore this case can be referred to as the magnetophoresis (MP) problem [3]. It is the subject of this paper. As we will frequently compare our findings with the more common case of the uniformly charged polymer, we will, for brevity, refer to the latter as the electrophoresis (EP) problem and to the present one as the MP problem, although the distinction between the two is not electromagnetic, but only in the forces exerted on the reptons (see Fig. 1).

The MP problem, within the framework of the Rubinstein–Duke model, has so far been studied by means of Monte Carlo simulations [3], and the calculations were mostly restricted to the drift velocity as function of the applied field and chain length. In this paper we analyze the MP problem by means of density-matrix renormalization-group (DMRG) techniques, which allow us to perform a detailed analysis of both global quantities as drift and curvilinear velocities and diffusion coefficient, but also on local average shapes of the polymer.

The dynamics of the reptating chain is governed by the Master Equation which we put in the form

$$\frac{\partial P(\mathbf{y}, t)}{\partial t} = \sum_{\mathbf{y}'} H(\mathbf{y}, \mathbf{y}') P(\mathbf{y}', t) \quad (1)$$

Here \mathbf{y} stands for the set of links y_1, \dots, y_{N-1} , where y_j measures the distance between the repton j and $j + 1$, along the direction of the applied field. In our lattice representation the y_j can take the values ± 1 and 0 . The value $y_j = 0$ corresponds to the case that the reptons j and $j + 1$ occupy the same cell. Thus each zero is a unit of stored length. The non-zero values represent the cases where $j + 1$ occupies a cell “higher” (1) or “lower” (-1) than j . Higher and lower refer to a position in the direction of the field. \mathbf{y} represents a complete configuration of the chain (see Fig. 1). $P(\mathbf{y}, t)$ is the probability distribution of the configuration at time t and the matrix $H(\mathbf{y}, \mathbf{y}')$ contains the gain and loss transitions from \mathbf{y}' to \mathbf{y} . The bias in the hopping rate is contained in the matrix elements of H . Generally we have for the bias factor

$$B_j = \exp(aq_j E/k_B T) \quad (2)$$

with q_j the charge of repton j , E the driving field, a the distance between adjacent cells (measured along the field direction) and $k_B T$ the standard combination of Boltzmann’s constant and the absolute temperature. In the MP problem all $q_j = 0$ except for $j = N$. We put

$$B_N \equiv B = \exp(\varepsilon/2) \quad (3)$$

and use ε as the parameter for the driving field. The other parameter of the model is the number of reptons N .

We have chosen this “hamiltonian form” of the Master Equation in order to stress the formal correspondence with a quantum mechanical model governed by a hamiltonian matrix. The DMRG method exploits this analogy and indeed its success in one-dimensional quantum problems carries over to reptation problems [4, 5, 6]. We are interested in the stationary state of the probability distribution. In the quantum language this corresponds to finding the right eigenvector of H belonging to the eigenvalue zero. The adaptation of the DMRG method to the MP problem is straightforward and the data presented in this paper are obtained by the DMRG method. An important difference with the Master Equation is that in

quantum mechanical problems the hamiltonian is hermitian, whereas in the reptation problem the matrix H is non-hermitian, due to the influence of the driving field. This restricts the applicability of the DMRG-method to moderately long chains and/or small driving fields.

The physics of the EP and MP problems is qualitatively different. As illustration consider the weak field case (ε small), where the Nernst–Einstein relation $v = FD$ relates the drift velocity v to the total applied force F and the diffusion coefficient D . The force F , equals $N\varepsilon$ in the EP case, since one pulls at each repton. It is well known that v scales as $v \sim \varepsilon/N$, yielding for the diffusion the non-trivial result $D \sim N^{-2}$. In the MP problem D will be essentially the same, as hopping is limited by the availability of stored length. In both cases the motion can be considered as diffusion of stored length. Since $F = \varepsilon$ in the MP problem, we expect the drift velocity to scale as $v \sim \varepsilon N^{-2}$, a feature which is born out by our calculations.

In the Sec. II we discuss some moment equations derived from the Master Equation which are more helpful than in the EP problem in analyzing the drift- and curvilinear velocity. They are expressed in terms of the probabilities n_j^k that the link j has the value $y_j = k$. The sum of the n_j^k adds up to 1

$$n_j^0 + n_j^+ + n_j^- = 1 \quad (4)$$

So it suffices to consider the two quantities n_j^0 and m_j defined by

$$n_j^0 = \langle 1 - y_j^2 \rangle \quad m_j = \langle y_j \rangle = n_j^+ - n_j^- \quad (5)$$

n_j^0 can be called the local density of stored length. m_j is a measure for the local orientation and will be referred to as the profile of the chain.

In the Sections III and IV we present our data for the velocities and the profiles. The analysis is most transparent in the strong field limit where we can make an ansatz which almost perfectly represents the data. In section IV we discuss the behavior of the profile for weak and strong pulling fields.

II. MOMENTS OF THE MASTER EQUATION

The DMRG method deals with the whole probability distribution $P(\mathbf{y})$. In the MP problem it is fruitful to consider moments of the Master Equation. One set of moments is obtained by multiplying Eq. (1) with y_j and then summing over all \mathbf{y} . This leads to $N - 1$ relations which can be seen as an expression of the fact that the drift velocity v across all the $N - 1$ links of the chain must be the same on the average. An even more useful set of relations is obtained by multiplying the Master Equation by y_j^2 and summing over all \mathbf{y} . The resulting $N - 1$ relations are an expression of the fact that the curvilinear velocity J is the same across all links. These

relations obtain the form

$$J = n_{j-1}^0 - n_j^0 \quad 1 < j < N \quad (6)$$

which can be viewed as the familiar law that the current J equals minus the gradient of the density of the stored length. In addition to Eq. (6) one has two relations [12] concerning the traffic in and out both ends of the chain. They read

$$\begin{aligned} J &= 1 - 3n_1^0, \\ J &= (n_{N-1}^0 - n_{N-1}^-)B + (n_{N-1}^0 - n_{N-1}^+)B^{-1} \end{aligned} \quad (7)$$

The expression for the drift velocity involves correlations between neighboring links

$$v = \langle (1 - y_{j-1}^2)y_j - (1 - y_j^2)y_{j-1} \rangle \quad (8)$$

and it is therefore not as informative as Eq. (6). As one sees Eq. (7) involves only averages over the first (last) link. This holds also for the expressions for the drift velocity in terms of the averages of the first and last link.

$$\begin{aligned} v &= m_1, \\ v &= (n_{N-1}^0 + n_{N-1}^-)B - (n_{N-1}^0 + n_{N-1}^+)B^{-1} \end{aligned} \quad (9)$$

These equations have been derived by Barkema and Schütz [3] using balance arguments.

Equation (6) is a powerful relation since it allows to express the density of stored length in terms of the curvilinear velocity

$$n_j^0 = n_1^0 - (j-1)J \quad (10)$$

showing that the density profile is linear in the position of the cell. In particular (10) implies a relation between the densities of the first and last cell

$$n_{N-1}^0 = n_1^0 - (N-2)J \quad (11)$$

We have used the linearity of the density n_j^0 as a check of the numerical calculations.

Counting the number of unknowns (v , J , n_1^0 , n_{N-1}^0 , m_1 , m_{N-1}) and the number of equations (7), (9) and (11) we see that we have one more unknown than equations. This situation is similar to the EP problem. There the expression for the curvilinear velocity does not obtain the simple form (6), due to the bias on the internal reptons. So one misses relation (11). On the other hand $J = 0$ for EP, due to the symmetry of the polymer on exchanging head and tail. Thus in both cases the moment equations are not sufficient to determine the velocities. Higher moments do not lead to additional information since again higher order correlations appear.

III. GLOBAL QUANTITIES

We discuss first the behavior of global quantities as the drift and curvilinear velocities and the diffusion constant.

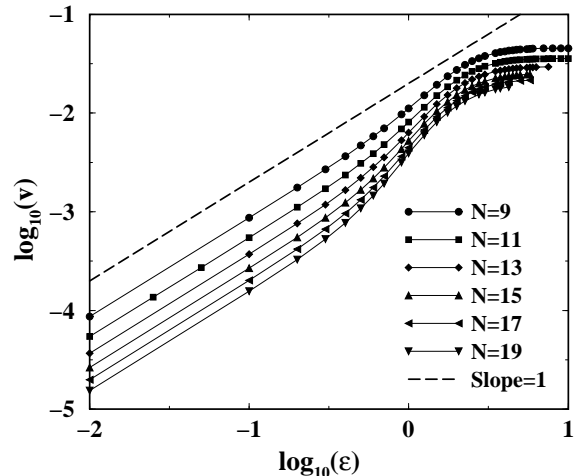


FIG. 2: Plot of $\log v$ vs. $\log \varepsilon$ for various N .

A. The Weak Field Limit

In the weak field limit the polymer assumes mostly a random configuration and all the densities n_j^k are close to $1/3$. The overall behavior of the drift velocity v as function of ε and N is given in Fig. 2. Note that the drift velocity becomes proportional to ε for small ε , as expected on the basis of the Nernst – Einstein relation discussed above. For stronger fields, the velocity saturates to a finite value, as discussed in the next paragraph. A similar dependence of v on ε and N was observed in the Monte Carlo study of Ref. [3]. The limiting behavior for small ε and large N is thus:

$$v(N) \sim \varepsilon D(N) \sim \frac{\varepsilon}{N^2}, \quad (12)$$

with $D(N)$ the zero field diffusion coefficient. The scaling behavior of $D(N)$ as function of the length N has been studied quite intensively [7, 8, 9, 10]. Reptation theory predicts that $D(N) \sim 1/N^2$, while conflicting results appeared on experimental measurements, for which both $1/N^2$ and, more recently, $1/N^{2.3}$ [11] have been reported.

A detailed study of the scaling of $D(N)$, within the Rubinstein–Duke model by means of DMRG method was recently performed [4, 5], for various end-point stretching rates. In that case the diffusion coefficient was calculated from the limiting value of the drift velocity for $\varepsilon \rightarrow 0$, with the field acting on all reptons (the EP problem). Here we repeat the same analysis only for a single case (using a stretching rate $d = 1$ following the definition of d of Refs. [4, 5]). The advantage of calculating $D(N)$ with a small field acting only on an end repton is that the DMRG procedure is much more stable in this case and one can compute longer chains. This is due to the fact that in the MP problem non-hermiticity is restricted only to the repton where the field is applied. As mentioned in the introduction non-hermiticity hampers the efficiency

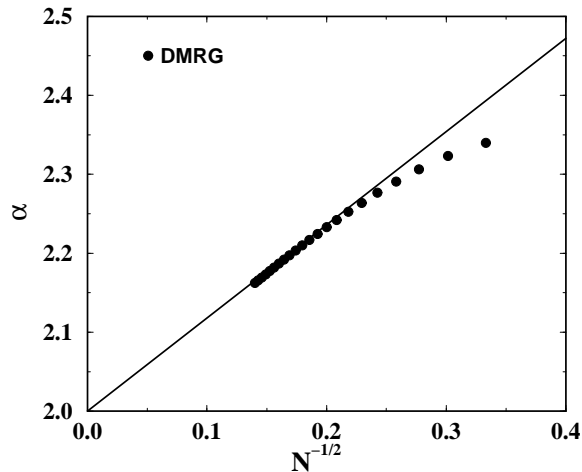


FIG. 3: Plot of the effective exponent $\alpha(N)$ calculated for $\varepsilon = 10^{-3}$ up to $N = 51$ from the decay of the diffusion coefficient $D(N)$ and plotted as a function of $1/\sqrt{N}$. The fact that $\alpha(N)$ approaches linearly the limiting value 2 supports the scaling form for the diffusion coefficient given in Eq.(13).

of the DMRG method.

In order to calculate the diffusion coefficient from the Nernst-Einstein relation $D = \lim_{\varepsilon \rightarrow 0} v/\varepsilon$ in practice, we used a small field ($\varepsilon = 10^{-3}$) and checked explicitly that results do not change for smaller fields. The scaling behavior of the diffusion coefficient is expected to be:

$$D(N)N^2 = A + \frac{A'}{\sqrt{N}} + \dots \quad (13)$$

with A and A' some constants. The form of the sub-leading correction to $D(N)$ has been debated for a while [13, 15] and recent DMRG results suggest that it is of the type $1/\sqrt{N}$ [4], supporting Eq. (13). The coefficient was determined exactly [14, 15, 16]: $A = 1/3$.

To analyze the scaling behavior of $D(N)$ it is most convenient to use the logarithmic derivative of the DMRG data:

$$\alpha(N) = -\frac{\ln[D(N)] - \ln[D(N+2)]}{\ln N - \ln(N+2)}, \quad (14)$$

which is shown for $N = 9, 11, \dots, 51$ in Fig. 3. Plugging Eq. (13) in Eq. (14) one finds for the effective exponent $\alpha(N) = 2 + A'/(2A\sqrt{N})$, a behavior which is accurately reproduced by our numerical data of Fig. 3. The present results corroborate previous claims [4] about the scaling form of $D(N)$.

B. The Strong Field Limit

In the strong field limit the polymer assumes an oriented configuration, with the '+' links dominating at the

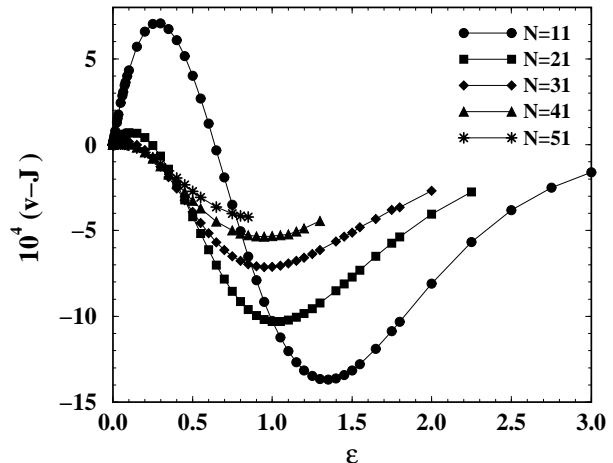


FIG. 4: Difference between the drift v and curvilinear J velocities as function of the applied field and for various chain lengths.

pulled end. At the other end we still have a substantial amount of links '0', since the polymer can only move by the diffusion of stored length from the tail to the head. Eliminating n_1^0 from Eq. (10) with the use of Eq. (7) we get

$$n_{N-1}^0 = \frac{1}{3}(1 - KJ), \quad (15)$$

where $K = 3N - 5$. In order that n_{N-1}^0 stays finite for $N \rightarrow \infty$, the curvilinear velocity must vanish as

$$J \sim K^{-1} \quad N \rightarrow \infty \quad (16)$$

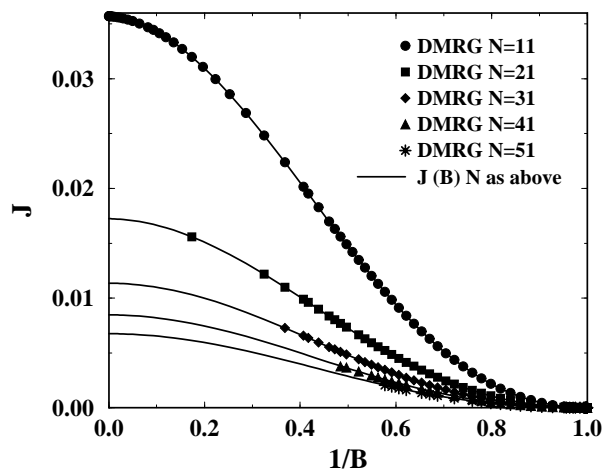


FIG. 5: Comparison between the DMRG data (symbols) and the crossover formula (solid lines) of Eq. (19) for the curvilinear velocity J .

As one sees from (15) this limiting value is not sufficient to determine the limiting value of density n_{N-1}^0 , which is sensitive to the corrections to (16). For the strong field limit it is useful to relate the drift velocity to the curvilinear velocity. With (7) and (8) we get

$$v = J + 2(n_{N-1}^- B - n_{N-1}^0 B^{-1}), \quad (17)$$

Now, if the polymer is fully stretched, v and J become the same. In Fig. 4 we have plotted the difference $v - J$ as calculated by DMRG for various fields and chain lengths. We note that it is small for all values of ε and N , in particular for strong fields and that this tendency is enforced for long polymers. That it also is small in the small field limit is a consequence of the fact that both quantities vanish in that limit. In order for the difference to vanish we must have

$$n_{N-1}^0 \simeq B^2 n_{N-1}^- \quad (18)$$

Now we may use this relation as the 6th relation, which enables us to make all the desired quantities explicit functions of ε and N . We find for instance

$$J(B) = v(B) = \frac{B^4 - 2B^2 + 1}{K(B^4 + B^2 + 1) + 3B^3}, \quad (19)$$

$$n_{N-1}^0(B) = \frac{1 + B/K}{B^2 + 1 + 3B/K + 1/B^2}. \quad (20)$$

This explicit field dependence is compared to the data in Fig. 5 and Fig. 6. The agreement is excellent in both cases. Note also that Eq. (19) is consistent with Eq. (16) and that it provides the proportionality coefficient.

However, the crossover formulae (19)-(20) do not describe the subtle dependencies in the limit of small fields $B = \exp(\varepsilon/2) \rightarrow 1$. In this limit the drift velocity vanishes as $v \sim \varepsilon$, while one observes from (19), that the curvilinear velocity vanishes as $J \sim \varepsilon^2$. For this reason, in the limit $\varepsilon \rightarrow 0$, the crossover formula (19) predicts $v \sim \varepsilon^2/(3N - 5)$, in disagreement with the correct scaling behavior of Eq. (12). The strong field limit does not suffer from this problem. We note, for instance, that in the limit $N \rightarrow \infty$ the saturation value of the velocity for $B \rightarrow \infty$ is in agreement with the exact expression given in Ref. [3]: $v = 1/(3N - 5)$.

IV. PROFILES

Next we discuss some profiles, *i.e.* the local orientation $m_i \equiv \langle y_i \rangle$ as function of the segment position along the chain. We consider $N - 1$ segments, thus N -reptons with the charged one at head position N . Fig. 7 shows a plot of m_i/ε as function of the scaled variable $(i - 1)/(N - 2)$ for chains of various lengths and at fixed field $\varepsilon = 0.001$. This profile corresponds to the linear regime where the drift velocity scales as $v \sim \varepsilon$. The notable feature is a symmetry between head and tail with respect to the center of the chain, although the magnetophoresis problem is clearly asymmetric. This symmetry can be shown

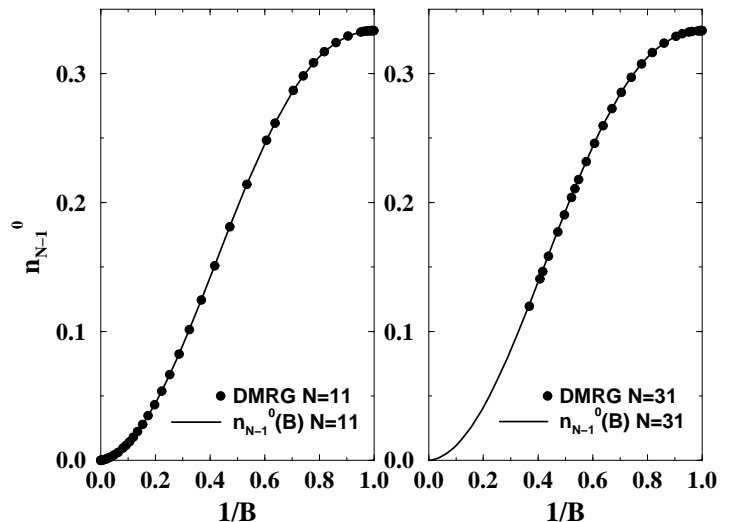


FIG. 6: Comparison between the DMRG data (symbols) and the crossover formula (solid lines) of Eq. (20) for n_{N-1}^0 .

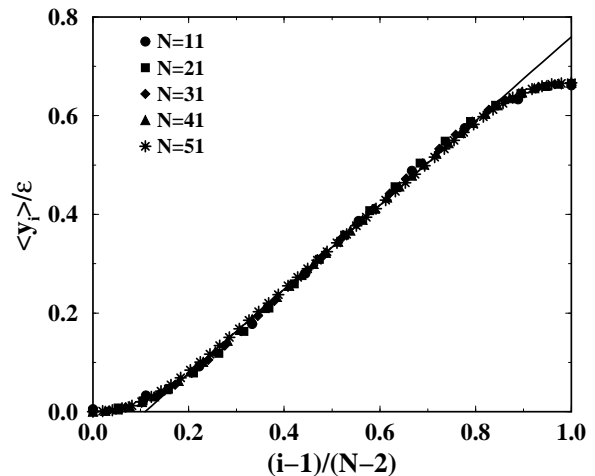


FIG. 7: Average profiles $\langle y_i \rangle/\varepsilon$ for various lengths and for $\varepsilon = 10^{-3}$.

[18] to be strict in the weak field limit. It disappears for stronger values of the field as Fig. 8 shows, where profiles are plotted for $\varepsilon = 1$ and various lengths N .

In order to analyze the data further we also plot the individual probabilities n_i^k for having a $+$, 0 or $-$ at the site i of the chain. For small values of ε (not shown here) the curves are all near $1/3$, with a slight excess of $+$ links at the head and a depletion of $-$ links. The densities of $+$ and $-$ links are monotonically increasing and decreasing functions of the position i . For intermediate fields $\varepsilon = 1$, the densities are more interesting and in Fig. 9 we plot the values of n_i^0 , n_i^+ and n_i^- for $N = 51$. The linear behavior for n_i^0 is consistent with Eq. (10). The curve for n_i^+ is monotonically increasing, but that for n_i^- is not monotonically decreasing.

The qualitative behavior of the orientation profile can be understood by considering the “origin” of the non-zero links ($y_i = \pm 1$) as has been introduced by Barkema and Newman [8]. In the MP problem more links are created at the pulled head than at the tail. They stream gradually down to the tail. We can keep track for every link $y_i = \pm 1$, whether it is formed at the head or at the tail. After sufficient time the chain is divided into two zones: a head zone and a tail zone. They are separated by a small intermediate region with zeroes (we do not follow the origin of the zeroes). The zones remain separated because the $y_i = \pm 1$, created at the head cannot cross the $y_i = \pm 1$ created at the tail. The division between the two zones fluctuates in time and occasionally the tail zone disappears, while very rarely (particularly at large fields) the head zone vanishes. The larger the force on the head, the larger the asymmetry between the head and tail zones. We supplement these speculations by making an assumption on the ratios

$$r_i(j) = p_i^+(j)/p_i^-(j) \quad (21)$$

where $p_i^\pm(j)$ is the probability of finding a \pm at i when the division is at j . We put

$$r_i(j) = r_h \quad \text{for } j < i \quad (22)$$

$$r_i(j) = 1 \quad \text{for } j \geq i \quad (23)$$

Since in the tail zone there is no distinction between $+$ and $-$ we have set the ratio equal to 1. The idea, underlying this assumption, is that the $+$ and $-$ links are interlocked. So while moving in their zone their ratio can not change.

At position i the average number of nonzero links ($+$ and $-$) is equal to $1 - n_i^0$. We introduce f_i as the fraction of such nonzero links which are in the head zone. One can express the densities n_i^\pm in terms of f_i as

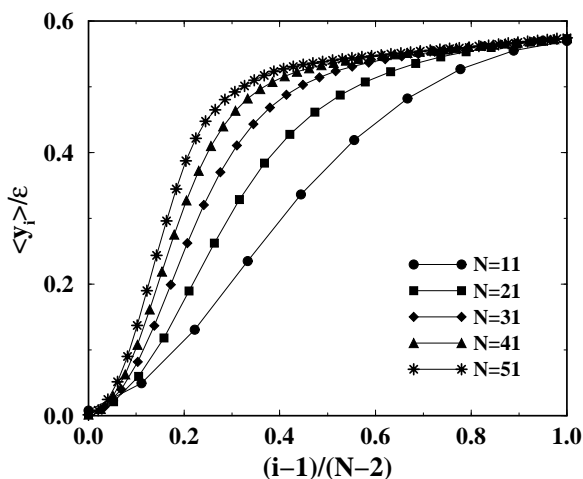


FIG. 8: As in Fig. 7 for $\epsilon = 1$.

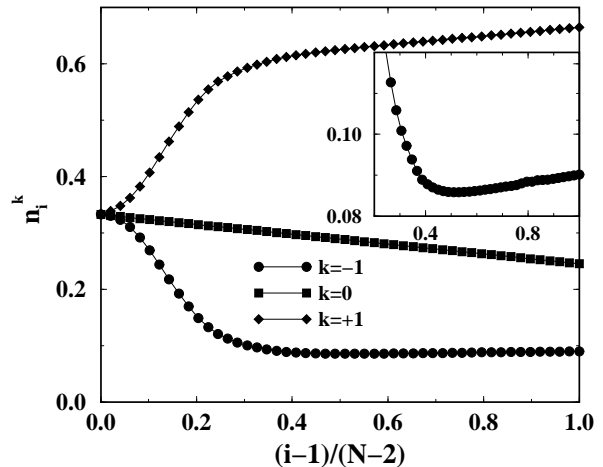


FIG. 9: Plot of the average densities $\langle n_i^+ \rangle$, $\langle n_i^0 \rangle$ and $\langle n_i^- \rangle$ for $\epsilon = 1$ and $N = 51$. Inset: Blow up of the density n_i^- , showing a non-monotonic behavior with a linear increase as function of i by approaching the pulled edge.

$$\begin{cases} n_i^+ = \left(f_i \frac{r_h}{r_h + 1} + (1 - f_i) \frac{1}{2} \right) [1 - n_i^0] \\ n_i^- = \left(f_i \frac{1}{r_h + 1} + (1 - f_i) \frac{1}{2} \right) [1 - n_i^0] \end{cases} \quad (24)$$

In both equations the terms proportional to f_i are the contributions that i is in the head zone while the terms proportional to $1 - f_i$ are the contributions from the case in which i is in the tail zone. We see that in the magnetophoresis problem the situation simplifies, since we do not have to worry about the tail zone. It drops out when we consider the profile

$$m_i = n_i^+ - n_i^- = \frac{r_h - 1}{r_h + 1} f_i [1 - n_i^0] \quad (25)$$

Thus the profile m_i is, apart from the known factor $1 - n_i^0$, directly related to the fraction f_i . The latter has a simpler interpretation. It starts out at $i = 1$ with a value nearly zero, since the head zone will only seldomly extend over the whole chain. It ends at $i = N - 1$ at a value very close to 1, since the tail zone will hardly ever extend over the whole zone. We can use this fact to tie the ratio r_h to the end point values, discussed earlier, by considering (25) for $i = N - 1$

$$\langle y_{N-1} \rangle = \frac{r_h - 1}{r_h + 1} [1 - n_{N-1}^0] \quad (26)$$

and solving for r_h . It leads to

$$\langle y_i \rangle = \langle y_{N-1} \rangle f_j \frac{1 - n_i^0}{1 - n_{N-1}^0} \quad (27)$$

This form contains only f_i as unknown. We can draw some conclusions from Eqs. (25) and (27) for weak fields, as well as for long chains at stronger fields.

A. Weak Fields

For $\epsilon \rightarrow 0$ we may put

$$r_h = 1 + a_h \epsilon \quad (28)$$

The function $1 - n_i^0$ will approach the limit $2/3$, so (25) becomes

$$\langle y_i \rangle = \epsilon \frac{a_h}{3} f_i \quad (29)$$

For the zero field limit of the profile we can take the zero field limit of f_i . It has the property that head and tail become equivalent or

$$f_i = 1 - f_{N+1-i} \quad \text{or} \quad f_i + f_{N+1-i} = 1 \quad (30)$$

The zero field limit of f_i has been determined in [8] by Monte Carlo simulations. We note that (30) is consistent with the mentioned [18] symmetry in $\langle y_i \rangle$. One should have $a_h = 2$ in order that the profile becomes $2\epsilon/3$ at the head, as is observed (see Fig. 7). This is perfectly in agreement with the value $r_h = B^4 \sim 1 + 2\epsilon$ for small ϵ . Combining (29) and the first Eq. (9) we find that f_1 is a measure for the drift velocity v . According to (12) f_1 should vanish as $1/3N^2$. This result has been derived in [8].

Another feature of Fig. 7 seems to be the collapse of the data on a single curve. Further data on longer chains show that the flattening-off at the ends of the chain shrinks with the size of the system and that the slope in the middle slowly decreases. This is another manifestation of the slow approach towards the asymptotic behavior [18] for large N .

Note that if the division between the head and tail region were located with equal probability on all sites of the chain then one would have simply $f_i = i/N$, which from Eq. (29) implies a linear profile. The profile of Fig. 7 is linear only at the center of the chain, while it strongly deviates from linearity close to the edges. This implies that the probability of finding the division between the head and tail regions is flat in the center of the chain and drops off at the chain edges.

B. Long Chains and stronger Fields

In this case the head zone will be dominant beyond a certain point (i.e. $f_i = 1$ for $i > i_0$) in the chain, thus

the division between the head and tail zones is expected to become localized close to the end of the chain which is not pulled. The curves in Fig. 9 convincingly show this behavior. It is interesting to note that when $f_i \rightarrow 1$, Eq. (24) becomes:

$$\begin{cases} n_i^+ = [1 - n_i^0] \frac{r_h}{r_h + 1} \\ n_i^- = [1 - n_i^0] \frac{1}{r_h + 1} \end{cases} \quad (31)$$

It immediately implies that both n_i^+ and n_i^- are linearly increasing functions of i in the head zone, being n_i^0 a linearly decreasing function of i (see Eq. (10)). This explains the monotonic increase of n_i^- close to the pulled end shown in the inset of Fig. 9. Note that using Eq. (31) one can estimate r_h from the ratio of the slopes of n_i^+ and n_i^- in the head region. We find a ratio $r_h \simeq B^4$ in agreement with our crossover formulae.

V. DISCUSSION

We have presented a series of numerical and analytical results for the MP problem in the Rubinstein - Duke model, where a single reptating polymer is pulled by a constant driving field applied to one polymer end. We have shown that the numerical data for the drift- and curvilinear velocities can be quite well reproduced by simple interpolating formulas following from the assumption that both velocities are equal in the limit of long chains. Indeed the measured differences are small which shows that the polymer is fairly stretched by the pulling force.

We studied also local quantities, as the profiles, which provide information on the shape of the reptating chain. These are quite well understood using a representation in which the polymer is divided into a head and tail region, with different ratios of + and - links. At small fields the division between the two regions meanders trough the whole chain, and the probability of finding it close to the edges drops off. At strong fields the division gets localized close to the free end of the chain. Moreover some profiles show an unexpected non-monotonic behavior which has a simple interpretation in the interface picture. The precise shape of the profiles at weak fields close to the polymer edges, both at finite N and in the asymptotic limit $N \rightarrow \infty$, will be discussed in details elsewhere [18].

Acknowledgements: This work has been supported by the Polish Science Committee (KBN) under grant in years 2003-2005. A.D. acknowledges a grant from the Royal Netherlands Academy of Science (KNAW) enabling him to stay at the Leiden University where part of this investigation were carried out.

[1] M. Rubinstein, Phys. Rev. Lett. **59**, 1946 (1987); T. A. J. Duke, Phys. Rev. Lett. **62**, 2877 (1989).

[2] J.-L. Viovy, Rev. Mod. Phys. **72**, 813 (2000); G. W.

- Slater *et al.*, Electrophoresis **23** 3791 (2002).
- [3] G.T. Barkema and G.M. Schütz, *Europhys. Lett.* **35**, 139 (1996).
- [4] E. Carlon, A. Drzewiński, and J. M. J. van Leeuwen, *Phys. Rev. E* **64**, R010801 (2001).
- [5] E. Carlon, A. Drzewiński, and J. M. J. van Leeuwen, *J. Chem. Phys.* **117**, 2435 (2002).
- [6] M. Paessens and G. M. Schütz, *Phys. Rev. E* **66**, 021806 (2002).
- [7] B. Widom, J.-L. Viovy and A. D. Defontaines, *J. Phys I France* **1**, 1759 (1991).
- [8] G. T. Barkema and M. E. J. Newman, *Physica A* **244**, 25 (1997).
- [9] G. T. Barkema and M. H. Krentzlin, *J. Chem. Phys.* **109**, 6486 (1998).
- [10] A. L. Frischknecht and S. T. Milner, *Macromolecules* **33**, 5273 (2000);
- [11] T. P. Lodge, *Phys. Rev. Lett.* **83**, 3218 (1999).
- [12] Elimination of J from the equations (6)-(7) gives the $N-1$ moment equations.
- [13] G. T. Barkema, J. F. Marko and B. Widom, *Phys. Rev. E* **49**, 5303 (1994).
- [14] J. M. J. van Leeuwen and A. Kooiman, *Physica A* **184**, 79 (1992).
- [15] M. Prähofer and H. Spohn, *Physica A* **233**, 191 (1996).
- [16] Michael Widom and I. Al-Lehyani, *Physica A* **244**, 510 (1997).
- [17] B. Derrida and M. R. Evans in *Nonequilibrium Statistical Mechanics in One dimension*, edited by V. Privman (Cambridge University Press, Cambridge, 1997); G. Schütz in *Phase transitions and critical phenomena* edited by C. Domb and J. Lebowitz (Academic, London 2000), vol. 19.
- [18] Shown in a forthcoming paper.